Fluctuating potentials in GaAs:Si nanowires: critical reduction of the influence of polytypism on the electronic structure

N. Ben Sedrine,*[a] R. Ribeiro-Andrade,[b,f] A. Gustafsson,[c] M. R. Soares,[d] J. Bourgard,[a] J. P. Teixeira,[a] P. M. P. Salomé,[b,e] M. R. Correia,[a] M. V. B. Moreira,[f] A. G. De Oliveira,[f] J. C. González,[f] and J. P. Leitão[a]

In this work, the effects of Si doping in GaAs nanowires (NWs) grown on GaAs (111)B by molecular beam epitaxy with different Si doping levels (nominal free carrier concentrations of $1x10^{16}$, $8x10^{16}$, $1x10^{18}$ and $5x10^{18}$ cm^{-3}) are deeply investigated using scanning electron microscopy (SEM), transmission electron microscopy (TEM), grazing incidence X-ray diffraction (GID), photoluminescence (PL) and cathadoluminescence (CL). TEM results reveal a mix of wurtzite (WZ) and zinc-blende (ZB) segments along the NWs' axis independently of the Si doping levels. GID measurements suggest a slight increase of the ZB fraction with the Si doping. Low temperature PL and CL spectra exhibit sharp lines in the energy range 1.41-1.48 eV, for the samples with the lower Si doping levels. However, the emission intensity increases and is accompanied by a clear broadening of the observed lines for the samples with the higher Si doping levels. The staggered type-II band alignment only determines the optical properties of the lower doping levels in GaAs:Si NWs. For the higher Si doping levels, the electronic energy level structure of the NWs is determined by electrostatic fluctuating potentials intimately related to the amphoteric behavior of the Si dopant in GaAs. For the heavily doped NWs, the estimated depth of the potential wells is ~ 96 - 117 meV. Our results reveal that the occurrence of the fluctuating potentials is not dependent on the crystalline phase and shows that the limitation imposed by the polytypism can be overcome.

Introduction

The unique properties of semiconductor nanowires (NWs), such as: large surface-to-volume ratio, possible quantum confinement effects, NW's diameter dependence of excitation and emission of electronic states, give these nano-building blocks an outstanding potential for electronic, photonic, mechanical, biological, and energy-conversion applications[1–3]. The NWs growth parameters influence the material composition, doping, and crystal quality, that will tailor their structural, electrical and optical properties which are relevant for potential applications[4]. In the particular case of arsenide-based NWs, such as GaAs NWs, one of the most troublesome properties is the control over their crystalline structure. It is well-known that most of these NWs are grown with polytypism consisting of the simultaneous occurrence of zinc-blende (ZB) and wurtzite (WZ) crystalline structures along the NW's axis[1]. Furthermore, the WZ structure is not stable in the bulk form of such semiconductors[5]. It was reported that the presence of polytypism has a strong influence on the electronic structure of the NWs as revealed by structural, electrical and optical measurements[5–9]. Doping is another crucial issue for the NW applications. As an example, it was recently reported that the doping in GaAs NWs, was able to increase the radiative efficiency with an ultrashort lifetime and deliver superior room temperature lasing performance, with respect to undoped and surface passivated GaAs/AlGaAs heterostructure NWs.[10] Indeed, n-type doping of GaAs can be realized with dopants like Te, S and Se, whereas doping with Be and Mg is responsible for p-type electrical conductivity[9,11–15]. Group IV atoms can occupy both cation and anion sites in III-V semiconductors, i.e., they possess an amphoteric behaviour. They are mainly shallow levels because their ionization energies are in the order of the thermal energy (k_BT, where k_B is the Boltzmann constant) enabling a significant ionization at room temperature. In the case of Si in the GaAs lattice, the atoms can be incorporated on Ga sites (Si_{Ga}) acting as donors or on As sites (Si_{As}) acting as acceptors, depending on several factors namely the silicon concentration, the substrate orientation, the growth temperature and the III-V flux ratio[16–21]. The measured ionization energies of Si in both sites of GaAs are 5.8 meV (Si_{Ga}) and 34.8 meV (Si_{As})[22,23]. In the literature, several works discussed the existence of a doping profile along the radius and along the axis

a. Departamento de Física and I3N, Universidade de Aveiro, Campus Universitário de Santiago, 3810-193 Aveiro, Portugal
b. INL - International Iberian Nanotechnology Laboratory, Quantitative Electron Microscopy, Avenida Mestre José Veiga, 4715-330 Braga, Portugal
c. Solid State Physics and NanoLund, Box 118, Lund University, Lund SE-22100, Sweden
d. Laboratorio Central de Analises, Universidade de Aveiro, 3810-193 Aveiro, Portugal
e. Departamento de Física, Universidade de Aveiro, Campus Universitário de Santiago, 3810-193 Aveiro, Portugal
f. Departamento de Física, Universidade Federal de Minas Gerais, 30123-970 Belo Horizonte, Minas Gerais, Brazil

https://doi.org/10.1039/C7NR08395E

for different types of NWs as a consequence of dopant incorporation from the side facets and/or from the liquid droplet[18,24–26].

As stated above, introducing dopant atoms is able to tune the semiconductor's optical and electrical properties. For low doping levels, it is possible to assume that the edges of both conduction and valence bands are constant along the semiconductor material. However, if the doping level is very high, the existence of high density of dopant atoms will promote the interaction between them[27] inducing a broadening of the donor or acceptor levels. This effect is even increased in the case of simultaneous occurrence of acceptor and donor states due to the occurrence of both types of ionized defects, thus, strongly dependent on the compensation level[28–31]. The degree of compensation of amphoteric dopants or auto-compensation increases at high doping levels, which results in a high density of ionized defects[32]. Due to the amphoteric role of Si in GaAs, a large incorporation of this dopant can potentially create electrostatic fluctuating potentials in the semiconductor, which can induce tails of the density of states inside the bandgap[27]. These fluctuations correspond to a change of the edges of both conduction and valence bands along the material. In this work, we study the effect of Si doping on the electronic structure of GaAs NWs grown on GaAs (111)B substrates by molecular beam epitaxy, with four nominal Si doping levels (nominal free carrier concentrations of $1x10^{16}$, $8x10^{16}$, $1x10^{18}$ and $5x10^{18}$ cm^{-3}). We demonstrate that the presence of fluctuating potentials in the samples with higher doping levels drastically decreases the influence of polytypism on the electronic structure, thus preventing the localization of charge carriers at the WZ/ZB interface.

Experimental details

Samples

Si-doped GaAs NWs were grown on GaAs (111)B substrates in a Riber 2300 R&D MBE reactor. The NWs growth was promoted through Au-assisted vapour-liquid-solid growth mechanism by drop-coating the substrate with Au colloidal nanoparticles (with average diameter of 5.0 ± 0.5 nm). The NWs growth was performed at 615°C, with an As_4 beam equivalent pressure (BEP) of $3.8x10^{-5}$ Torr, a Ga BEP of $7.2x10^{-7}$ Torr and at a nominal growth rate of 1 monolayer (ML)/s (estimated for an epitaxial layer). The in-situ Si doping was achieved by keeping the Si effusion cell at the temperatures: 820, 950, 1040 and 1100 °C for the samples A, A*, B and B*, respectively. A nominal free carrier concentration of $1x10^{16}$, $8x10^{16}$, $1x10^{18}$ and $5x10^{18}$ cm^{-3} was estimated for the samples A, A*, B and B*, respectively, by Hall effect measurements in GaAs thin films grown under the same conditions.

PL

Photoluminescence (PL) measurements were performed using a Bruker IFS 66v Fourier Transform Infrared (FTIR) spectrometer equipped with a liquid nitrogen cooled Ge detector. The samples were inserted in a helium flux cryostat that allowed changing the temperature from 5 to 300 K. The 514.5 nm line of an Ar^+ laser was used as excitation wavelength, and focused on the sample with a long focal length lens, with a spot diameter of ~1 mm, allowing to probe several hundred of NWs simultaneously. The excitation power was measured near the entrance window of the cryostat, and was changed in the range 1.25–118.00 mW for sample A, 0.46–77.80 mW for sample A*, 0.0013–2.01 mW for sample B, and 0.2–56.4 mW for sample B*. In average, lower excitation power values were used for sample B, in comparison with samples A, A* and B*, since its intense luminescence caused the saturation of the Ge detector for excitation power values above ~ 2 mW.

CL

Spectrally resolved cathodoluminescence (CL) was performed in a dedicated scanning electron microscope at low temperature (8 K) using a Si charge-coupled device (CCD) for hyper spectral imaging and a GaAs photomultiplier tube (PMT) for monochromatic imaging and single wavelength spectra. The cut-off of the PMT limits the lower energy detection to ~1.36 eV. An acceleration voltage of 5 kV was used with a probe current of 10-50 pA. The average spectra in figure 2 was recorded with the beam scanning over an area of about 50x70 μm^2, of the as grown samples using the PMT. For the hyperspectral imaging in figure 3, NWs were transferred to Si substrates by gently pushing the Si-substrate onto the as-grown NW substrate. This approach gives a high density of NWs, but low enough to allow for the selection of an individual NW for the imaging.

TEM

The NW microstructure was assessed by High-resolution Transmission electron microscopy (HRTEM) carried out with Jeol-JEM 2100 80-200 kV microscope operating at 200 kV. The specimen for TEM studies were obtained after scrapping out mechanically the NWs from the substrate, which were then deposited on a lacey carbon grid.

GID

The crystal structure of the samples was obtained by grazing incidence X-ray diffraction (GID) using the Cu-Kα1 radiation (λ = 1.540598 Å) from a PANalytical X'Pert MRD (additional details could be found in Ref.[9]). The GID measurements were performed with low incidence angles (ω = 0.1 to 1.5°, with steps of 0.2 below 1°, and 0.5 above 1°) in the 2θ range of 25° - 30°.

Results and discussion

Luminescence at low temperature

Figure 1 shows a comparison of the normalized PL spectra of samples A, A*, B and B* (with nominal free carrier concentrations of $1x10^{16}$, $8x10^{16}$, $1x10^{18}$ and $5x10^{18}$ cm^{-3}, respectively) acquired under similar experimental conditions: 5 K and laser power excitation of ~2 mW. First, we have verified for all samples that no measurable luminescence is recorded from the GaAs epilayer grown beneath the NWs, which allows us to conclude that it has no influence on the sample's luminescence.

The PL spectra comparison of the four samples reveal a few changes in their luminescence. It is found that the PL intensity of sample A is more than one order of magnitude lower when compared to the other three samples, which is also observed from the much higher signal-to-noise ratio for sample A. Furthermore, the luminescence of this sample shows narrow radiative transitions with dominant peak energies at ~1.418 and ~1.483 eV, and a full width at half maximum (FWHM) values of 7 and 20 meV, respectively.

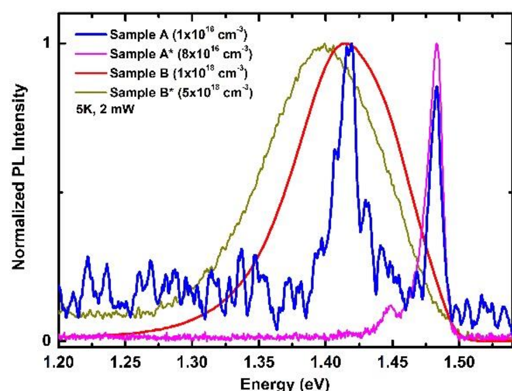

Fig. 1: Normalized PL spectra measured at 5 K of Si-doped GaAs NWs ensemble for samples A, A*, B and B* using an excitation power of ~2 mW.

For the second doping level (sample A*), the luminescence is dominated by the transition at ~1.483 eV, with a slight increase of the FWHM. Thus, both samples A and A* evidence similarities in the luminescence. On the other hand, a further increase in the doping level shows a noticeable change in the radiative de-excitation channels. For samples B and B*, the luminescence is dominated by an asymmetric and broad band (FWHM higher than 80 meV in both samples), and with peak energy in the range ~1.40-1.42 eV. Therefore, from the point of view of radiative recombination channels, the measured luminescence shows roughly two sets of samples with different behaviours: i) samples A and A* and ii) samples B and B*. Finally, it should be mentioned that no significant luminescence is observed for all four samples at energies below ~1.3 eV.

In the particular case of samples A and A*, the ones with sharper transitions, the comparison of the peak energies with the literature can be performed. According to Pavesi and Guzzi[33], who reported the main photoluminescence lines measured at 2 K in bulk GaAs, the well resolved emission observed at ~1.483 eV for sample A (and A*) can be either related to a transition from the conduction band to a neutral Si acceptor (1.485 eV) or from a neutral donor to a neutral Si acceptor (1.482 eV). On the other hand, Williams and Elliott[34] reported in Si-doped GaAs grown on Si(111), an emission peak at 1.417 eV which was associated to a Si_{As}-V_{As} complex. The nature of the radiative transitions will be further discussed below. Concerning the broader bands observed for the samples B and B* with the highest doping levels, the previous comparison is not possible due to the high FWHM values.

The observed differences in the luminescence, namely the significant increase of the FWHM and the merging of the sharp radiative transitions towards an asymmetric band by increasing the Si doping level, are rather intriguing. For these reasons, two issues should be addressed: i) confirm the luminescence results using a different technique; ii) investigate if the increase of the doping level is responsible or not for a significant structural change in the NWs. Therefore, a deeper study is performed on the two samples A and B, one from each set (stated above), with rather different optical properties. Hereafter, the study will be mainly focused on the analysis and discussion of these samples A and B, however additional optical results of samples A* and B* will be presented in Supplementary Information and in due time mentioned in the text in order to support the conclusions.

In order to verify the results obtained by PL, CL measurements were performed on samples A and B, at 8 K, for an accelerating voltage of 5 kV and a beam current of ~25 pA (Fig. 2). The measured CL spectra from the NWs ensemble indicate that: i) sample A shows narrow radiative transitions with peak energies at ~1.42 and ~1.49 eV; ii) sample B exhibits a broad luminescence with peak energy at ~1.44 eV; iii) the CL intensity is more than two orders of magnitude higher for sample B compared to sample A. Therefore, PL and CL results suggest that the radiative de-excitation channels studied by both techniques are similar despite the different excitation mechanisms, a laser for PL and an electron beam for CL. Similarly to PL, the influence of the GaAs epilayer on the NWs related luminescence for both samples must be discarded, because the luminescence from the epilayer is observed in a different energy range (see Fig. SI1 in Supplementary Information).

It is worth mentioning that both PL and CL spectra do not present any significant emission related to the ZB GaAs excitonic transition at 1.519 eV[35], and that all the radiative transitions at low temperature are occurring below ~1.5 eV.

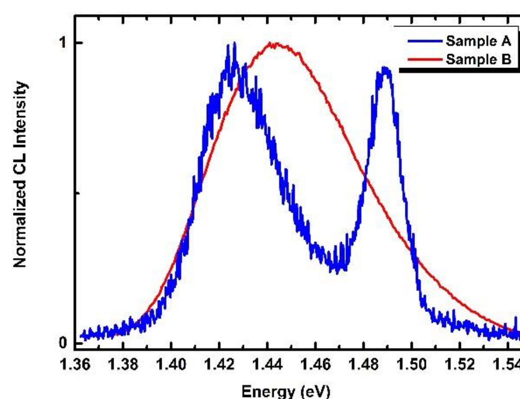

Fig. 2: Normalized CL spectra measured at 8 K of Si-doped GaAs NW ensemble. The used accelerating voltage is 5 kV, while the used current is 25 pA for sample A, and 20 pA for sample B.

The observed broadening of the luminescence with the increase of the Si doping, as seen for sample B, was previously reported in Si-doped GaAs NWs[36] and epilayers[21]. A similar behaviour was observed with other dopants, such as Te in GaAs epilayers[37] and Sn-doped shell in InP core-shell NWs[38]. In addition, an increase of the PL intensity, with more than two orders of magnitude, was demonstrated upon Zn doping of unpassivated GaAs NWs[10] and obtained in the n-type segments of GaAs NWs[39].

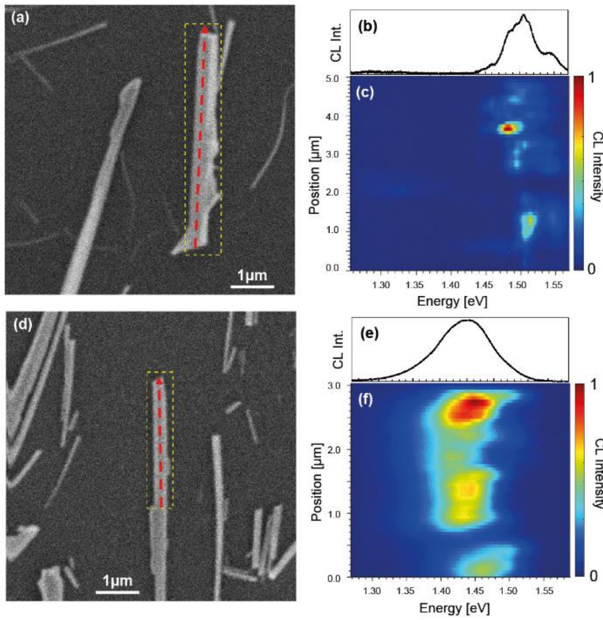

Fig. 3: Low-temperature hyperspectral CL images of individual Si-doped GaAs NWs: (a-c) Sample A and (d-f) sample B. (c) and (f) are the hyperspectral spectra of the NWs marked by the dashed yellow rectangle in (a) and (d), where the red arrows indicate line direction. (b) and (e) are the corresponding average spectra of the area in the yellow rectangle.

Low temperature hyperspectral CL spectra on individual NWs were also acquired. Figs. 3 (c) and (f) represent the hyperspectral spectra of the NWs marked by the dashed yellow rectangle in the SEM images (a) and (d), where the red arrows indicate line direction, and (b) and (e) are the corresponding average spectra, for samples A and B, respectively. The hyperspectral CL maps clearly show broader spectral and spatial luminescence for sample B (Fig. 3 (f)) with respect to sample A (Fig. 3 (c)). In other words, while in sample A the luminescence is dominated by a peak with FWHM of less than 50 meV (centered at ~1.49 eV), sample B shows a broader emission ~100 meV (centered at ~1.43 eV). These results reinforce the previous observations from PL and CL measured on an ensemble of NWs (Figs. 1 and 2, respectively). Furthermore, the apparent dimensions of the emitting regions are much smaller in sample A (width below ~500 nm) compared to sample B in which they are of a few µm.

As stated above, since the optical results (from PL and CL) show drastic modifications in the radiative de-excitation channels induced by the increase of the Si doping, it is important to explore if the structural properties of the GaAs NWs are also influenced by the Si doping.

Structural characterization

Representative SEM images of all the NW samples are shown exemplary for sample A in Supplementary Information (Fig. SI2). The NWs appear in dense regions with lengths up to several tens of micrometers. The diameters vary along the axis from a few hundreds of nanometers at the base to a few tens of nanometers at the tip. The SEM images (in Fig. SI2 a) show different orientations of the NWs with a slight predominance of vertical NWs for the short ones and non-vertical for the longer ones. No noticeable influence of the chemical nature of the dopant and doping level on the morphology could be recorded.

Figure 4 shows representative TEM, selected area electron diffraction (SAED) and HRTEM images of two single Si-doped GaAs NWs, selected from more than ten investigated NWs from samples A and B. Figs. 4 (a) and (b) reveal the presence of stacking faults with the characteristic mix of ZB and WZ segments, as well as twinned ZB segments, i.e. ZB [1,-1,0], ZB*[-1,1,0] and WZ [1,1,-2,0][6,40]. The SAED patterns in Figs. 4 (c) and (d) confirm the existence of atomic planes in both crystalline phases. HRTEM images of a typical region of the NWs are shown in Figs. 4 (e) and (f), in which the atomic segments are represented in yellow, green and cyan for ZB [1,-1,0], ZB*[-1,1,0] and WZ [1,1,-2,0], respectively.

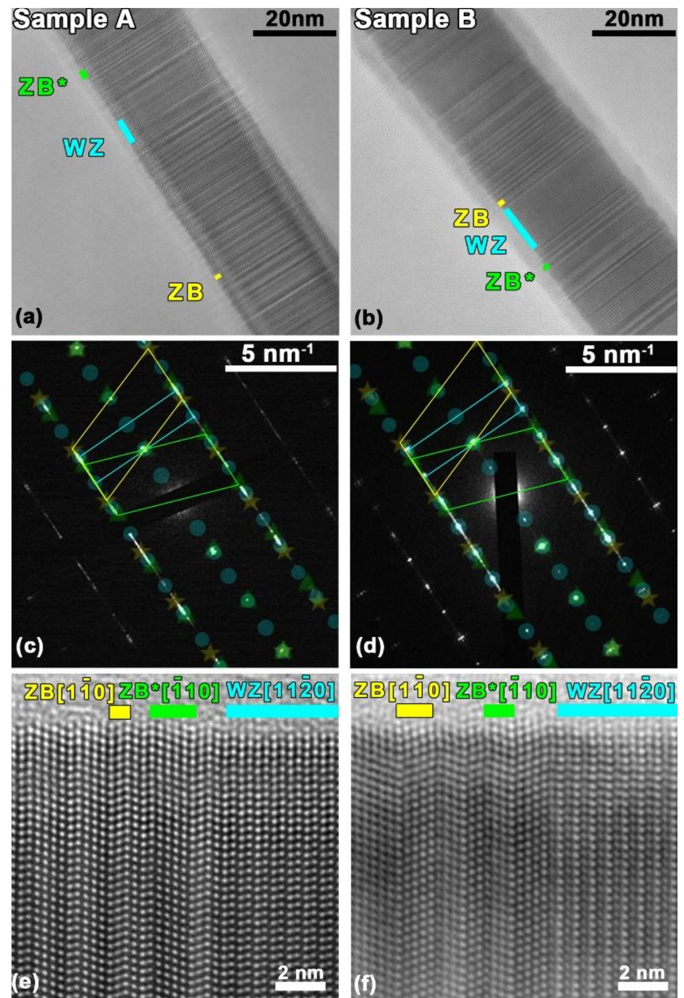

Fig. 4: TEM images (a and b), SAED patterns (c and d), and HRTEM images (e and f), of the Si-doped GaAs NWs sample A and sample B, respectively. The atomic segments are shown in yellow, green and cyan for ZB [1,-1,0], ZB* [-1,1,0] and WZ [1,1,-2,0], respectively.

Polytypism commonly occurs in III-V semiconductors at the interfaces between the two crystalline phases characterized by a step-like transition at the atomic scale as, for example, previously reported in GaAs[5,41,42] and InP[43,44]. For both samples A and B, Figs. 4 (a) and (b) show a clear polytypism with no evident dependence of the WZ/ZB fraction on the Si doping levels. The measurements performed in different NWs from samples A and B, revealed

similar results (see Fig. SI3 of Supplementary Information). Despite that, it should be noticed that TEM is a local technique unable to provide a significant statistical result, since only small regions of the NWs are probed and only a limited number of NWs could be measured (more than ten NWs in this work).

The TEM structural analysis of the NWs was complemented with GID measurements in order to give additional information regarding the possible presence of both ZB and WZ crystalline phases. We emphasize that GID measurement cannot provide information about the presence of polytypism (i.e. width of the ZB and WZ segments in the NWs). In order to minimize any contribution from the epilayer underneath the NWs to the X-ray diffraction signal, GID measurements were realized (for more details see Ref. 9). The diffractograms are presented in Figs. 5 (a) and (b) for samples A and B, respectively. In both cases, the patterns in the 2θ range of 25° - 30° are composed of three reflection peaks: P_I (2θ~25.8°), P_{II} (2θ~27.2°) and P_{III} (2θ~29.2°). In the studied 2θ range, the available information from the International Centre for Diffraction Data (ICDD)* predicts the observation of: *i)* one peak related with the ZB (111) planes near the P_{II} peak, and *ii)* three peaks related with WZ planes near the P_I, P_{II} and P_{III} peaks, with relative foreseen intensities of 999, 568 and 613, respectively. It should be emphasized that the WZ crystal structure has never been reported for GaAs films, and was only recorded in GaAs NWs. Therefore, P_I and P_{III} can be assigned to reflections from the WZ planes (10-10) and (10-11)† in the NWs, respectively. However, for P_{II}, both contributions from the WZ (0002) and ZB (111) planes, should be considered*. The observation of WZ planes other than the growth ones can be understood from the occurrence of different growth orientations of the NWs as shown by cross section SEM images in Fig. SI2 of Supplementary Information.

The WZ phase is only observed for GaAs NWs while the ZB phase could originate both from GaAs NWs and/or from the GaAs epilayer beneath the NWs. The relative intensity of peaks P_I and P_{III} assigned to the WZ GaAs phase exhibits a very small decrease when reducing the incidence angle, showing that the amount of WZ phase probed, is only slightly reduced by decreasing the incidence angle ω. At the same time, the intensity of the peak P_{II} decreases significantly, however, its relative intensity is always higher compared to the P_I and P_{III} WZ-related peaks, even for ω= 0.1°. For such ω value, the comparison of the relative intensities of P_I, P_{II} and P_{III} peaks with respect to the ones predicted for the WZ crystalline phase (values presented above), shows that the experimental relative intensity of peak P_{II} (higher than the ones of P_I and P_{III}) can only be explained by assuming the existence of ZB segments in addition to WZ in the NWs. Indeed, in Fig. 5 we included short dash dotted lines corresponding to WZ GaAs (0002) and ZB GaAs (111) reflections in GaAs nanowires[45], at 27.13° and 27.30°, respectively. Although no evident separation of the peaks is observed in our GID diffractograms (only of ~0.17° as reported by Jahn *et al.*[45]), our results are in accordance with the literature[1,41,42,45,46] and with the direct observation of both phases in TEM (Fig. 4). Finally, it should be emphasized that peak P_{II} exhibits a different dependence on ω for samples A and B: as ω decreases, a stronger decrease of the relative intensity of P_{II} is observed for sample A in comparison with sample B. This behaviour could be interpreted *a priori* as a slightly lower WZ/ZB ratio in sample B, however, further detailed and quantitative investigations of the WZ/ZB ratio and crystallographic texture are needed.

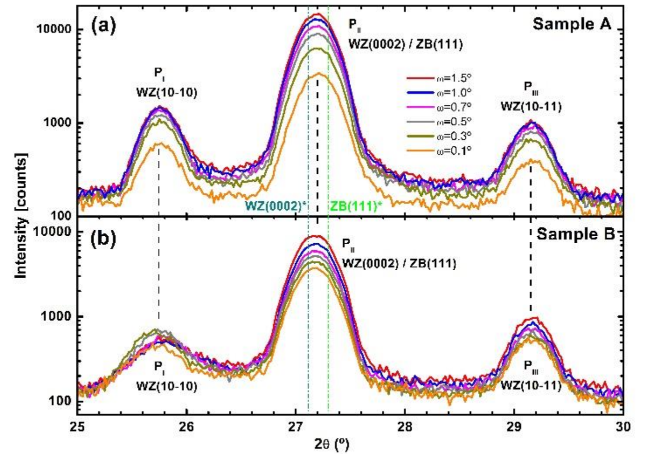

Fig. 5: GID diffractograms (ω/2θ scans) obtained for incidence angles ω ranging from 0.1° to 1.5° for samples A (a) and B (b). The indexation of each peak to the atomic planes in each crystalline phase is also shown. Black dashed lines indicate the position of P_I, P_{II} and P_{III} peaks. * Short dash dotted lines correspond to WZ GaAs (0002) (dark cyan) and ZB GaAs (111) (green) reflections peaks from Ref.[45].

PL excitation power and temperature dependences

The influence of the Si doping level on the electronic structure of the NWs can be analysed through the investigation of the PL dependencies on the excitation power and temperature. Due to the contribution of different radiative transitions to the PL spectra (Fig. 1), it is needed to perform a deconvolution of the peaks. The deconvolution procedure and data analysis are detailed in Supplementary Information (Fig. SI4). For sample A, the set of PL spectra, measured as a function of excitation power and temperature, verifies that the Gaussian components (A1, A2, A3 and A4) can be interpreted as independent radiative transitions. Nevertheless, the experimental results strongly suggest the observation of only two radiative transitions for sample B (component B4 and a transition denoted by B').

To investigate the nature of the radiative transitions observed for the NWs with different Si doping levels, PL excitation power dependence was performed at 5 K. The different signal-to-noise ratio in the PL spectra and the saturation limit of the detector induced different excitation power ranges for both samples. Independently of the Si doping level, the GaAs NWs were found to exhibit an increase of the PL intensity with increasing the excitation power as shown by the experimental points in Fig. 6. The dependence of the integrated PL intensity (I) on the normalized excitation power (P) can be parametrized by using the power law[47]:

$$I \propto P^m, \qquad (1)$$

where m is an adjustable parameter. Values of m~1 separates the case of excitonic (free or bound) transitions (m>1) from the case of transitions involving charge carriers with some degree of localization (m<1) as for free-to-bound transitions, donor-acceptor pair (DAP) recombination or type-II transitions. The best-fit values of the m parameters of all components are summarized in Table 1. The obtained m values are clearly lower than 1 for sample A and closer to 1 for sample B.

Regarding sample A, the values suggest a strong localization of the charge carriers. The polytypism in III-V NWs results in a staggered type-II band alignment at the WZ/ZB interface. In the case of GaAs NWs, under excitation and due to Coulomb interaction, the electrons (holes) are located in the ZB (WZ) side of the interface[1,5,45,48,49]. Consequently, the dominant radiative recombination channel should be the spatially indirect recombination of the carriers located in the two sides of the interface[5–9]. For nanostructures exhibiting type-II transitions, the reported *m* values are found to be lower than 1: 0.66-0.83 in Si/Ge quantum dots[50–52] and 0.8 in polytypic GaN NWs[53]. For sample A, the estimated *m* values are in accordance with a dominant effect of the polytypism on the nature of the radiative de-excitation channels for such low Si doping level, and are compatible with reported values for Mg doped GaAs NWs[9]. Sample A* shows similar *m* values as the ones for sample A (see Fig. SI5 (a) in Supplementary Information). On the other hand, for sample B, the values of *m* are significantly higher and closer to 1. In addition, the broad and asymmetric shape of the luminescence is quite different from the sharp transitions reported for a strong influence of the polytypism. Therefore, such behaviour suggests that a different dominant effect, other than polytypism, is responsible for the radiative de-excitation channels in this sample B. Sample B* with the highest Si doping level also shows a similar behaviour as sample B (see Fig. SI5 (a) in Supplementary Information).

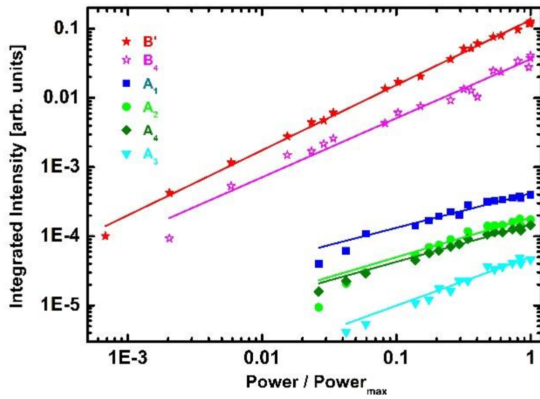

Fig. 6: Dependence on the excitation power of the relative intensity of the radiative transitions in Si-doped GaAs NW ensembles for samples A and B, measured at 5 K. B' and B_4 (A_1 to A_4) correspond to the radiative transitions identified for sample B (A). The lines represent the fit of Eq. (1) to each set of experimental points and the best-fit values are summarized in Table 1.

Table 1: Parameters obtained from the fit of Eqs. (1) and (2) to the experimental points obtained at 5 K, and resulting from the dependence on the excitation power of the relative intensities and peak energies, respectively, of the radiative transitions in samples A and B.

	Radiative transition	Energy (eV)	*m*	β (meV)
Sample A	A1	1.418	0.50±0.03	0.7±0.1
	A2	1.442	0.57±0.05	0.7±0.1
	A3	1.472	0.70±0.06	0.5±0.1
	A4	1.483	0.54±0.03	0.2±0.1
Sample B	B'	1.417	0.94±0.01	16.3±0.2
	B4	1.451	0.85±0.03	6.5±0.5

Normalized PL spectra as a function of excitation power are shown in Fig. 7. When the excitation power increases by two orders of magnitude, radically different behaviours are observed for the two Si doping levels. For sample A (Fig. 7 (a)), no apparent shift is observed for all radiative transitions, while for sample B (Fig. 7 (b)), the broad luminescence blue-shifts by ~123 meV in the studied excitation power range (0.0013-2.01 mW) with no significant change of the broadening. The apparent blue-shift of the broad luminescence for sample B cannot be related to a change of the relative intensities of the different transitions, as demonstrated in detail by the Gaussian component fits performed in all PL spectra as a function of the excitation power (see Fig. SI6 in Supplementary Information). Again, these results suggest a quite different nature of the radiative transitions in the NWs as a function of the different Si doping levels.

If the polytypism explanation is assumed, it is expected that an increase of excitation power results in a blue-shift[9]. However, the shift of ~123 meV observed for sample B is much higher than the one expected for type-II radiative transitions. It was recently reported that the increase of the Mg doping in GaAs NWs results in a deviation from a polytypic-related behaviour of the radiative transitions[54].

In order to quantify the blue-shift and further investigate the radiative de-excitation channels, the peak energies of the radiative transitions versus the excitation power are presented in Fig. 8 (a) for both samples. The dependence on the excitation power of the peak energy (*E*) of a transition can be described using[55–57]:

$$E = \beta . \ln\left(\frac{P}{P_0}\right), \qquad (2)$$

where β is a coefficient describing the energy shift and P_0 a fitting parameter. The best-fit values of β parameter of the different components are shown in Table 1. It is found that the energy shift values obtained for all radiative transitions in sample A are below 1 meV. Similar values were obtained for sample A* (see Fig. SI5 (b) in Supplementary Information). These values show the localization of carriers[55], which is also compatible with type-II transitions. Regarding sample B, the estimated β values are much higher than 1, namely ~16 and ~6 meV for the transitions B' and B_4, respectively. In the case of sample B*, the estimated β value (7.8±0.2 meV) is clearly higher than 2 meV (see Fig. SI5 (b) in Supplementary Information). β values of the same order of magnitude were reported by Yu in Be, Zn, Cd and Mg-implanted GaAs substrates for high carrier concentrations and high degree of compensation[55]. For lightly doped and relatively uncompensated GaAs, the value of β was found to be < or ≈2 meV. Another way to estimate the energy shift as a function of the excitation power is to use the shift per decade. Indeed, we have found values of ~38 and ~15 meV/decade, for B' and B_4, respectively. These values are comparable with the blue-shift of 24 meV/decade reported by Svavarsson *et al.*[20] for Si-doped GaAs films. Similar high β values are commonly reported in other semiconductors used in solar cells applications, such as $Cu_2ZnSn(S,Se)_4$ and $Cu(In,Ga)Se_2$[31,56–62]. These materials are characterized by electrostatic fluctuating potentials created by very high doping and compensation levels, inducing a strong influence on the radiative de-excitation channels which are different from the ones observed in lightly doped semiconductors[27].

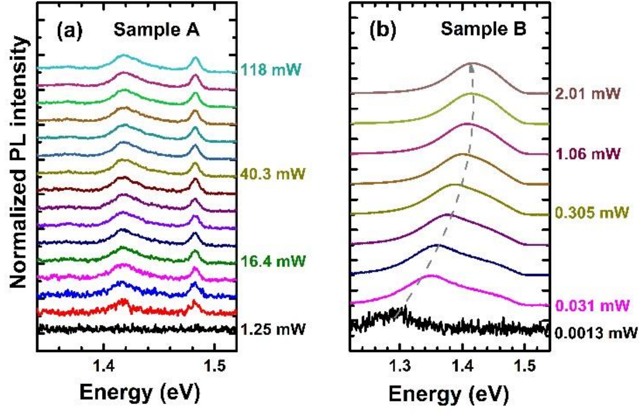

Fig. 7: Dependence on the excitation power of the normalized PL spectra of Si-doped GaAs NW ensembles for samples A (a) and B (b). The spectra are vertically shifted for clarity.

It is known that a shift of the peak energy depends on the type of band line-up alignment present in the system. It was demonstrated that for type-I heterostructures, the exciton transition energy is independent of the excitation power[63] or presents a blue-shift[64,65]. However, type-II transitions show a blue-shift of the peak energy as a function of the cubic root of the excitation power [9,66,67]:

$$E \propto P^{1/3} \quad (3)$$

Several reports demonstrated that the above blue-shift is compatible with type-II transition at the WZ/ZB interface of GaAs[5,9,68,69], InP[43,68] and GaN[53] NWs. In order to tentatively evaluate which observed radiative transitions are compatible with type-II transitions, the peak energies are plotted against the cubic root of the excitation power in Fig. 8 (b). As mentioned in the Experimental Details section, we remind that the used excitation power ranges are different for both samples, therefore resulting in non-superimposed experimental data points in Fig. 8 (b). Despite the very small blue-shift (below 1 meV) of the four radiative transition peak energies for sample A, the values show a linear dependence on $P^{1/3}$ in accordance with eq. (3). This result is compatible with type-II transitions. Nevertheless for sample B, a huge non-linear blue-shift is observed for B' and B_4. Consequently, for sample B with high Si doping, the electronic energy levels structure is not strongly affected by the polytypic structure of the NWs. Indeed, we notice that while the structural study by TEM suggests the occurrence of abrupt interfaces created by twins, stacking faults, and WZ/ZB alternated segments along the axis of the NW, the optical study suggests, on the contrary, some other dominant influence on the electronic structure that blurs the staggered type II band alignment at the WZ/ZB interface. Our results are in accordance with a recent report on Te-doped GaAs NWs[70]. The obtained high blue-shift values for sample B are typical for highly doped and strongly compensated semiconductors. It is also compatible with the observed shape of the emission: broad and asymmetric. A similar shape described by a quasi-exponential increase at the low-energy side and a steeper decrease at the high-energy side, was reported for different semiconductors, namely Cu-poor chalcopyrites and kesterites[56–60,71,72], Ge[29], GaAs[20], and ZnO NWs[73]. The shape of the band for sample B will be further discussed below.

Fig. 9 represents the dependence on temperature of the PL peak energy, measured at excitation power values of 100 and 2 mW for samples A and B, respectively. The temperature dependence of the bandgap energy of ZB GaAs, also shown in Fig. 9, was calculated using an equation proposed by Pässler and the corresponding ZB GaAs related parameters[74]. It can be seen that for sample A, all the radiative transitions roughly follow the trend of the bandgap energy of ZB GaAs. It is worth noting that the luminescence is only observed up to 60 K. On the other hand, for sample B, the two transitions shift to lower energies at a higher rate than the trend of the bandgap energy of ZB GaAs. Furthermore, their thermal quenching occurs for higher temperatures reaching up to ~110 K for the dominant transition. The two behaviours observed for both samples reinforces the differences regarding the nature of the radiative transitions for the low and high Si doping levels.

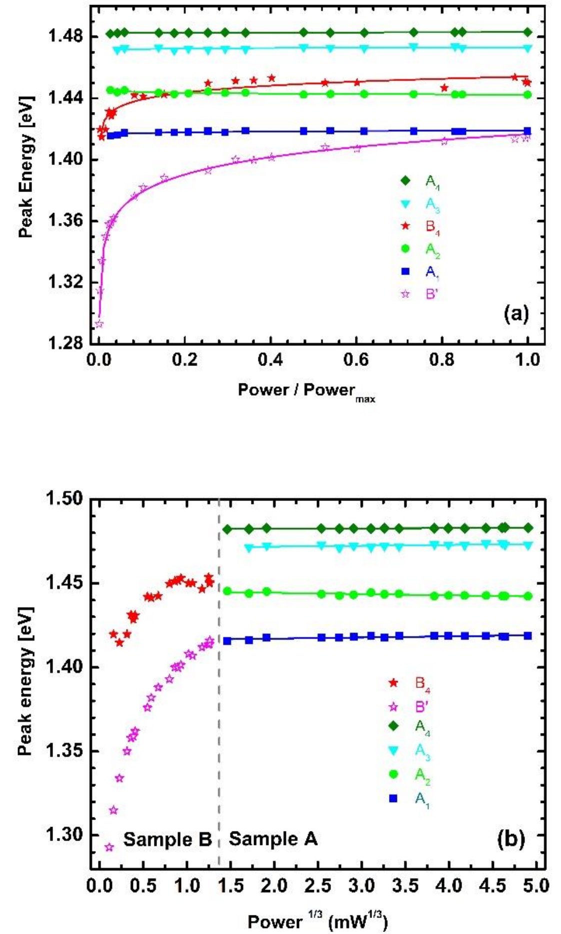

Fig. 8: Dependence on the excitation power P (a) and on $P^{1/3}$ (b), of the radiative transition peak energy of the Si-doped GaAs NW ensemble for samples A and B. Solid lines represent the best fit using eq. (2) (a) and eq. (3) (b). The best-fit values of Fig. 8 (a) are summarized in Table 1.

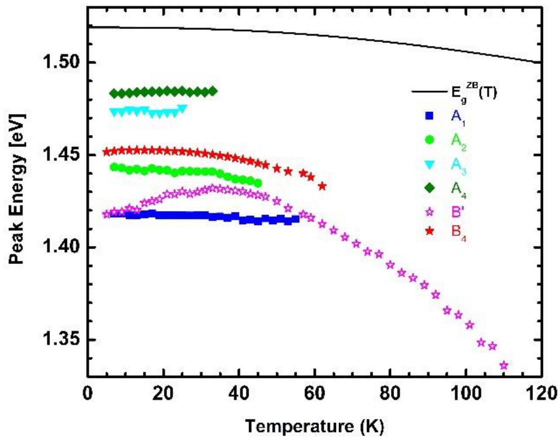

Fig. 9: Dependence on the temperature of the radiative transition peak energy, measured using excitation powers of 100 and 2 mW for samples A and B, respectively. The temperature dependence of the bandgap energy of ZB GaAs is shown (full line), calculated using eq. (17) in Ref.[74] and the corresponding ZB GaAs parameters.

It is known that fluctuating potentials can cause a red-shift of the PL due to the particular processes of charge carrier localization in tails or acceptor levels[27,28]. Contrarily to DAP transitions which usually exhibit a blue-shift with increasing temperature[71,72,75], transitions involving fluctuating potentials can exhibit a blue-shift and/or a red-shift[27,31].

Discussion

The structural and optical analysis of GaAs:Si NWs mainly demonstrated the following results: i) independently of the Si doping level, the NWs have the characteristic polytypism of the simultaneous occurrence of WZ and ZB segments; ii) the radiative de-excitation channels observed for the low Si doping levels are compatible with type-II transitions; iii) for the higher Si doping levels, no influence of the staggered type-II band alignment is observed on the radiative de-excitation channels. Therefore, these results evidence that the staggered type-II band alignment is not the dominant effect determining the electronic structure in the highly doped GaAs NWs, as it is the case for low doping levels. A possible explanation of our results is proposed below.

It is well known that Si is an amphoteric dopant in GaAs. By increasing the doping level, a higher density of ionized defects will be present in the material[27]. Actually, the observed dependence on the excitation power and temperature of the peak energy of the radiative transitions for sample B is typical for highly doped and strongly compensated materials[55]. The longer luminescent segments observed in CL suggest a similar amphoteric behaviour of Si in ZB and WZ GaAs. For these materials, depending on the density of ionized defects, a strong interaction occurs for $Na_B{}^3 \gg 1$, where *N* is the doping concentration of each type of defects, donors or acceptors, and a_B is the Bohr radius of the donor or acceptor states, respectively. Since the effective mass of the electrons is usually lower for electrons than for holes, the Bohr radius is larger for donor states in comparison with acceptor states. Thus, the interaction between donors have a higher influence on the creation of electrostatic fluctuating potentials in comparison with acceptors[31,76]. These fluctuations correspond to a change of the conduction and valence band edges along the material. Due to the differences in the interaction between the two types of defects, electrons can be bound in potential wells of the conduction band but not in discrete donor energy levels, whereas holes can be bound in potential wells of the valence band as well as in acceptor energy levels that follow the edge of the valence band[27]. Thus, the dynamics of charge carriers is strongly influenced by these electrostatic fluctuating potentials. This behaviour should be the same for both types of segments, WZ or ZB. Thus, such high density of ionized defects create electrostatic fluctuating potentials in both the WZ and ZB segments. This type of fluctuations keep the same bandgap energy inside a segment of a particular phase, and are associated with the appearance of tail states inside the bandgap. The root-mean-square depth of the potential wells created by the density of ionized defects is given by [27]:

$$\gamma = \sqrt{2\pi}\frac{e^2}{4\pi\epsilon r_0}\sqrt{N r_0{}^3}, \qquad (4)$$

where ε is the dielectric permittivity of the semiconductor, r_0 the screening radius, and *N* the total concentration of ionized donors and acceptors. The fluctuations are observed in the real space since the density of ionized defects is a function of the space coordinates. In Fig. 10 (a), a model describing the electrostatic fluctuating potentials in a highly doped and compensated NW is presented, in which the NW growth direction is considered along the Z axis. Perpendicularly to the Z axis of a particular segment (ZB or WZ), the fluctuating potentials occur similarly to bulk materials, as illustrated in Fig. 10 (a) for an arbitrary radial direction, R. Due to the fluctuating potentials occurring inside each of the ZB and WZ segments, the band alignment at the WZ/ZB interface is no longer well defined as for lightly doped materials (see Fig. 10 (b)). Furthermore, the effect of band alignment is only to shift the overall fluctuations in one segment relatively to the other, therefore the assumption of type-II transition is no longer applicable in this case. For clarity sake, in Fig. 10 (a), we only represent a very small interface region along the axis of the NW. Nevertheless, for a large enough thickness of the segments (ZB or WZ) along the Z axis, fluctuating potentials should also be present in that direction. Thus, with the occurrence of fluctuating potentials inside the segments, the effect of the band alignment expected from the polytypism in the NWs disappears. From the point of view of electronic structure in highly doped and compensated NWs, the alternation of ZB and WZ segments (polytypism) represents another (small) contribution to the occurrence of fluctuating potentials but is not the dominant effect for the creation of fluctuating potentials. In the case of the presence of a doping profile along the radius or the axis of the NW, the depth of the potential wells should change accordingly in such directions, which could be reflected in Fig. 10 (a). However, the experimental data presented in this work do not give any hint about a possible doping profile.

An additional issue must be discussed. In the literature, the reported offsets of the conduction and valence bands at the WZ/ZB interface are in the range ~50 - 120 meV[77–79]. Our results imply that the staggered type II band alignment is softened by the fluctuating potentials. This can be accomplished if the depth of the fluctuating potentials is high enough. In order to confirm this hypothesis, we performed the fit of the broad band luminescence intensity in the low energy side using equations corresponding to different types of radiative transitions[27,80,81]. This energy region is only related with the radiative transition B' (see Fig. SI4 in Supplementary Information). The obtained best-fit model, represented in Fig. 11, corresponds to a band-tail type transition, for which the energy dependence is described by[80]:

$$I(E) \propto \left(\frac{\gamma^2}{E_g - E}\right)^{\frac{3}{2}} exp\left(-\frac{(E_g - E)^2}{2\gamma^2}\right), \quad (5)$$

where γ is the depth of the fluctuating potentials and E_g is the bandgap energy of the doped semiconductor. It is known that the exact WZ GaAs bandgap is still controversial, and could be equal[82] or different[83] from the ZB GaAs bandgap. Furthermore, the E_g values depend on the doping level[14]. Therefore, in order to estimate the depth of the fluctuating potentials in sample B using eq. 5, we have assumed that the E_g value is the one of undoped ZB GaAs (1.519 eV at low temperature). The estimated γ value for sample B is 96 ± 1 meV, which is in accordance with our assumption that the depth of the fluctuating potentials is high enough to soften the staggered type II band alignment created by the polytypism. The best-fit model obtained for sample B* is presented in Fig. SI7 in Supplementary Information, and the estimated γ value is 117.3 ± 0.4 meV, which is higher than the one for sample B, and compatible with larger electrostatic fluctuating potentials, in agreement with its larger doping level.

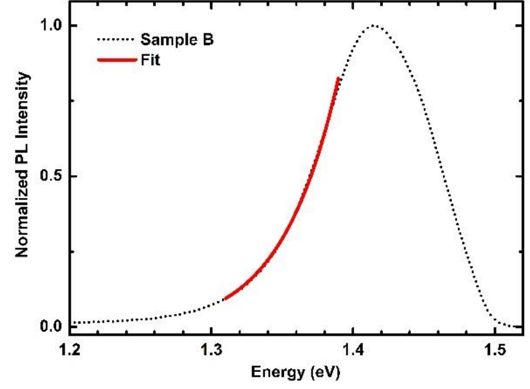

Fig. 11: Estimation of the depth of the fluctuating potentials for sample B, γ = 96 ± 1 meV. The PL spectrum was measured at 5 K (presented in Fig. 1) and the red solid line represents the fit with eq. (5) in the range 1.31–1.39 eV.

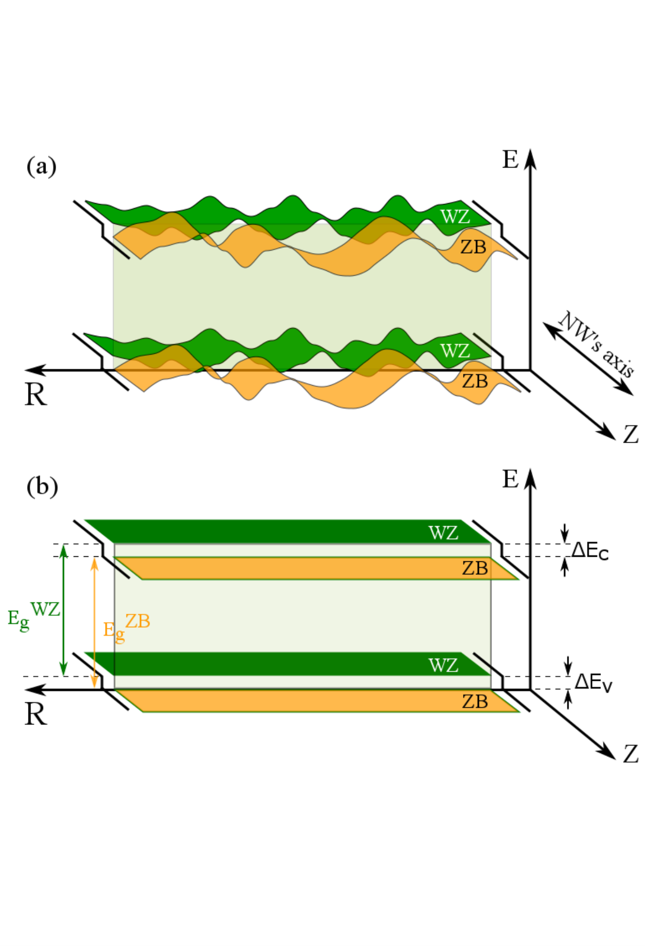

Fig. 10: Electronic structure for highly doped and compensated (a), and lightly doped (b) NW materials. Z represents the growth direction of the NW whereas R is an arbitrary radial direction perpendicular to Z axis. ΔE_c and ΔE_v are the conduction and valence bands offsets at the WZ/ZB interface, respectively, in the lightly doped NW.

Having fluctuating potentials inside each segment, the relative importance of the band offsets at the WZ/ZB interface decreases and the localization of charge carriers at that interface is no longer the dominant contribution determining the electronic energy levels structure of the NW. The doping represents a possible approach to overcome the limitations in their electrical and optical properties introduced by the occurrence of polytypism in NWs. We must note that, even with the existence of fluctuating potentials, some types of semiconductors like chalcopyrites and kesterites, used as absorber layer in solar cells, allow competitive device performance in comparison with similar devices based on mono and poly-crystalline Si, CdTe, etc, which are actually references in the photovoltaic market. Thus, the occurrence of fluctuating potentials is not a fundamental obstacle for applications of such highly doped GaAs NWs, but at the opposite, can represent a step towards the III-V NW optoelectronic applications.

Conclusions

In summary, the effect of Si doping in GaAs NWs on the structural and electronic properties, was deeply investigated for different Si doping levels (nominal free carrier concentrations of $1x10^{16}$, $8x10^{16}$, $1x10^{18}$ and $5x10^{18}$ cm^{-3}). With the increase of the Si doping level, a remarkable increase of the luminescence intensity was observed as well as an apparent decrease of the WZ/ZB fraction ratio. We have found that ZB/WZ polytypism only affects the electronic energy levels structure of the NWs with low Si doping levels. In the face of the amphoteric behaviour of Si in the GaAs lattice, a high doping results in high density of ionized defects which create electrostatic potential fluctuations in the conduction and valence band edges as well as tails of the density of states inside the bandgap. The radiative and non-radiative de-excitation channels change accordingly and the polytypism is no more the dominant effect determining the charge carriers dynamics. The estimated depth of the fluctuations is in the range 96-117 meV. The electronic structure of highly Si-doped GaAs NWs as well as the increase of the luminescence intensity open up new optoelectronic applications based on III-V NWs.

Conflicts of interest

There are no conflicts of interest to declare.

Acknowledgements

This work was funded by FEDER funds through the COMPETE 2020 Programme and National Funds through FCT - Portuguese Foundation for Science and Technology under the projects UID/CTM/50025/2013, and by the Brazilian agencies CNPq, FAPEMIG and CAPES. The CL work was performed with support from the Swedish research council (VR). P. M. P. Salomé acknowledges the funding of Fundação para Ciência e Tecnologia (FCT) through the project IF/00133/2015.

Notes and references

1 H. J. Joyce, Q. Gao, H. H. Tan, C. Jagadish, Y. Kim, J. Zou, L. M. Smith, H. E. Jackson, J. M. Yarrison-rice, P. Parkinson and M. B. Johnston, *Prog. Quantum Electron.*, 2011, **35**, 23–75.

2 N. P. Dasgupta, J. Sun, C. Liu, S. Brittman and S. C. Andrews, *Adv. Mater.*, 2014, **26**, 2137–2184.

3 M. Fang, N. Han, F. Wang, Z. Yang, S. Yip, G. Dong, J. J. Hou, Y. Chueh and J. C. Ho, *J. Nanomater.*, 2014, **702859**, 1.

4 C. Thelander, P. Agarwal, S. Brongersma, J. Eymery, L. F. Feiner, A. Forchel, M. Scheffler, W. Riess, B. J. Ohlsson and L. Samuelson, *Mater. Today*, 2006, **9**, 28–35.

5 D. Spirkoska, J. Arbiol, A. Gustafsson, S. Conesa-Boj, F. Glas, I. Zardo, M. Heigoldt, M. H. Gass, A. L. Bleloch, S. Estrade, M. Kaniber, J. Rossler, F. Peiro, J. R. Morante, G. Abstreiter, L. Samuelson and A. Fontcuberta I Morral, *Phys. Rev. B - Condens. Matter Mater. Phys.*, 2009, **80**, 245325.

6 N. Cifuentes, E. R. Viana, H. Limborço, D. B. Roa, A. Abelenda, M. I. N. Silva, M. V. B. Moreira, G. M. Ribeiro, A. G. De Oliveira and J. C. González, *J. Nanomater.*, 2016, 9451319.

7 A. C. S. Pimenta, D. C. T. Ferreira, D. B. Roa, M. V. B. Moreira, A. G. De Oliveira, M. De Giorgi, D. Sanvitto and F. M. Matinaga, *J. Phys. Chem. C*, 2016, **120**, 17046.

8 I. Zardo, F. Peiro, J. R. Morante, J. Arbiol, E. Uccelli and G. Abstreiter, *Phys. Rev. B - Condens. Matter Mater. Phys.*, 2009, **80**, 245324.

9 B. P. Falcão, J. P. Leitão, M. R. Correia, M. R. Soares, F. M. Morales, J. M. Mánuel, R. Garcia, A. Gustafsson, M. V. B. Moreira, A. G. De Oliveira and J. C. González, *J. Appl. Phys.*, 2013, **114**, 183508.

10 T. Burgess, D. Saxena, S. Mokkapati, Z. Li, C. R. Hall, J. A. Davis, Y. Wang, L. M. Smith, L. Fu, P. Caroff, H. H. Tan and C. Jagadish, *Nat. Commun.*, 2016, **7**, 11927.

11 A. K. Rai, R. S. Bhattacharya, P. P. Pronko, A. K. Rai, R. S. Bhattacharya and P. P. Pronko, *Appl. Phys. Lett.*, 1982, **41**, 1086.

12 C. E. C. Wood, D. Desimone, K. Singer, G. W. Wicks, E. C. Wood, D. Desimone, K. Singer and G. W. Wicks, *J. Appl. Phys.*, 1982, **53**, 4230.

13 B. P. Falcão, J. P. Leitão, J. C. González, M. R. Correia, K. G. Zayas-Bazan, F. M. Matinaga, M. B. Moreira, C. F. Leite and A. G. De Oliveira, *J. Mater. Sci.*, 2013, **48**, 1794–1798.

14 B. P. Falcão, J. P. Leitão, M. R. Correia, M. F. Leitão, M. R. Soares, M. V. B. Moreira, A. G. de Oliveira, F. M. Matinaga and J. C. González, *J. Mater. Chem. C*, 2014, **2**, 7104.

15 N. Cifuentes, H. Limborço, E. R. Viana, D. B. Roa, A. Abelenda, M. I. N. da Silva, M. V. B. Moreira, G. M. Ribeiro, A. G. de Oliveira and J. C. González, *Phys. Status Solidi b*, 2016, **253**, 1960–1964.

16 N. Sakamoto, K. Hirakawa and T. Ikoma, *Appl. Phys. Lett.*, 1995, **67**, 1444.

17 M. Hilse, M. Ramsteiner, S. Breuer, L. Geelhaar and H. Riechert, *Appl. Phys. Lett.*, 2010, **96**, 10–12.

18 J. Dufouleur, C. Colombo, T. Garma, B. Ketterer, E. Uccelli, M. Nicotra and A. Fontcuberta, *Nano Lett.*, 2010, **10**, 1734–1740.

19 C. Colombo, M. Heiss, M. Grätzel and A. F. Morral, *Appl. Phys. Lett.*, 2009, **94**, 173108.

20 H. G. Svavarsson, J. T. Gudmundsson, G. I. Gudjonsson and H. P. Gislason, *Phys. Scr.*, 2002, **T101**, 114.

21 M. K. Hudait, P. Modak and S. B. Krupanidhi, *Mater. Sci. Eng. B*, 1999, **56**, 1–11.

22 S. M. Sze and K. N. Kwok, *Physics of Semiconductor Devices*, 2006.

23 G. Oelgartt, G. Lippoldf, M. Proctor, D. Martin and F. K. Reinhart, *Semicond. Sci. Technol.*, 1991, **6**, 1120.

24 E. C. Garnett, Y. Tseng, D. R. Khanal, J. Wu and J. Bokor, *Nat. Nanotechnol.*, 2009, **4**, 311.

25 D. E. Perea, E. R. Hemesath, E. J. Schwalbach, J. L. Lensch-falk, P. W. Voorhees and L. J. Lauhon, 2009, **4**, 315–319.

26 C. Rolland, P. Caroff, C. Coinon, X. Wallart and R. Leturcq, *Appl. Phys. Lett.*, 2013, **102**, 223105.

27 A. P. Levanyuk and V. V Osipov, *Sov. Phys. Usp*, 1981, **24**, 187.

28 B. I. Shklovskii and A. L. Efros, *Electronic Properties of Doped Semiconductors*, Springer S., 1984.

29 V. P. Dobrego, I. S. Shlimak and P. Dobrego, *Phys. Status Solidi*, 1969, **33**, 805–809.

30 Z. I. Alferov; V. M. Andreev; D. Z. Garbuzov; and M. K. Trukan, *Sov. Phys. Semicond.*, 1973, **6**, 1718.

31 J. P. Teixeira, R. A. Sousa, M. G. Sousa, A. F. Da Cunha, P. A. Fernandes, P. M. P. Salomé and J. P. Leitão, *Phys. Rev. B - Condens. Matter Mater. Phys.*, 2014, **90**, 235202.

32 E. F. Schubert, *Doping in III-V Semiconductors*, Cambridge University Press, 1993.

33 L. Pavesi and M. Guzzi, *J. Appl. Phys.*, 1994, **75**, 4779–4842.

34 E. W. Williams and C. T. Elliott, *J. Phys. D. Appl. Phys.*, 1969, **2**, 1657–1665.

35 J. Melorose, R. Perroy and S. Careas, *Phys. Rev. B*, 1972, **6**, 3750–3753.

36 A. Suzuki, T. Mori, A. Fukuyama, T. Ikari, J. H. Paek and M. Yamaguchi, *Jpn. J. Appl. Phys.*, 2011, **50**, 06GH08.

37 J. Desheng, Y. Makita, K. Ploog and H. J. Queisser, *J. Appl. Phys.*, 1982, **53**, 999.

38 D. Lindgren, O. Hultin, M. Heurlin, K. Storm, M. T. Borgström, L. Samuelson and A. Gustafsson, *Nanotechnology*, 2015, **26**, 45705.

39 D. Sager, C. Gutsche, W. Prost, F. J. Tegude and G. Bacher, *J. Appl. Phys.*, 2013, **113**, 174303.

40 H. J. Joyce, J. Wong-leung, Q. Gao, H. H. Tan and C. Jagadish, *Nano Lett.*, 2010, **10**, 908.

41 D. Spirkoska, A. L. Efros, W. R. L. Lambrecht, T. Cheiwchanchamnangij, A. F. Morral and G. Abstreiter, *Phys. Rev. B - Condens. Matter Mater. Phys.*, 2012, **85**, 45309.

42 C. Wilhelm, A. Larrue, X. Dai and C. Soci, *Nanoscale*, 2012, **4**, 1446–1454.
43 N. Akopian, G. Patriarche, L. Liu, J. C. Harmand and V. Zwiller, *Nano Lett.*, 2010, **10**, 1198–1201.
44 R. L. Woo, R. Xiao, Y. Kobayashi, L. Gao, N. Goel, M. K. Hudait, T. E. Mallouk and R. F. Hicks, *Nano Lett.*, 2008, **8**, 4664.
45 U. Jahn, J. Lähnemann, C. Pfüller, O. Brandt, S. Breuer, B. Jenichen, M. Ramsteiner, L. Geelhaar and H. Riechert, *Phys. Rev. B - Condens. Matter Mater. Phys.*, 2012, **85**, 45323.
46 A. Biermanns, S. Breuer, A. Davydok, L. Geelhaar and U. Pietsch, *J. Appl. Crystallogr.*, 2012, **45**, 239–244.
47 T. Schmidt, K. Lischka and W. Zulehner, *Phys. Rev. B*, 1992, **45**, 8989–8994.
48 K. A. Dick, P. Caroff, J. Bolinsson, M. E. Messing, J. Johansson, K. Deppert, L. R. Wallenberg and L. Samuelson, *Semicond. Sci. Technol. 25*, 2010, **25**, 24009.
49 N. Vainorius, D. Jacobsson, S. Lehmann, A. Gustafsson, K. A. Dick, L. Samuelson and M. E. Pistol, *Phys. Rev. B - Condens. Matter Mater. Phys.*, 2014, **89**, 165423.
50 R. Apetz, L. Vescan, A. Hartmann, C. Dieker and H. Lüth, *Appl. Phys. Lett.*, 1995, **66**, 445.
51 M. W. Dashiell, U. Denker, C. Müller, G. Costantini, C. Manzano, K. Kern, O. G. Schmidt, G. Costantini and C. Manzano, 2006, **1279**, 10–13.
52 Y. Chen, B. Pan, T. Nie, P. Chen, F. Lu, Z. Jiang and Z. Zhong, *Nanotechnology*, 2010, **21**, 175701.
53 G. Jacopin, L. Rigutti, L. Largeau, F. Fortuna, F. Furtmayr, F. H. Julien, M. Eickhoff and M. Tchernycheva, *J. Appl. Phys.*, 2011, **110**, 64313.
54 P. Kannappan, N. Ben Sedrine, J. P. Teixeira, M. R. Soares, B. P. Falcão, M. R. Correia, N. Cifuentes, E. R. Viana, M. V. B. Moreira, G. M. Ribeiro, A. G. De Oliveira, J. C. González and J. P. Leitão, *Beilstein J. Nanotechnol.*, 2017, **8**, 2126–2138.
55 P. W. Yu, *J. Appl. Phys.*, 1977, **48**, 5043–5051.
56 J. P. Teixeira, R. A. Sousa, M. G. Sousa, A. F. Da Cunha, P. A. Fernandes, P. M. P. Salomé, J. C. González and J. P. Leitão, *Appl. Phys. Lett.*, 2014, **105**, 163901.
57 J. P. Teixeira, R. A. Sousa, M. G. Sousa, A. F. Da Cunha, P. A. Fernandes, P. M. P. Salomé, J. C. González and J. P. Leitão, *Appl. Phys. Lett.*, 2015, **107**, 163901.
58 J. P. Leitão, N. M. Santos, P. A. Fernandes, P. M. P. Salomé, A. F. Cunha, J. C. González and F. M. Matinaga, *Thin Solid Films*, 2011, **519**, 7390–7393.
59 T. Gokmen, O. Gunawan, T. K. Todorov, D. B. Mitzi, T. Gokmen, O. Gunawan, T. K. Todorov and D. B. Mitzi, *Appl. Phys. Lett.*, 2013, **103**, 103506.
60 J. P. Leitão, N. M. Santos, P. A. Fernandes, P. M. P. Salomé, A. F. Cunha, J. C. Gonzalez, G. M. Ribeiro and F. M. Matinaga, *Phys. Rev. B*, 2011, **84**, 24120.
61 M. Lang, C. Zimmermann, C. Krämmer, T. Renz, C. Huber, H. Kalt and M. Hetterich, *Phys. Rev. B*, 2017, **95**, 155202.
62 K. Tanaka, Y. Takamatsu, S. Miura, I. Cu, S. Katagiri and E. The, *phys. stat. sol. c*, 2017, **14**, 1600138.
63 L. Rigutti, M. Tchernycheva, A. De Luna Bugallo, G. Jacopin, F. H. Julien, F. Furtmayr, M. Stutzmann, M. Eickhoff, R. Songmuang and F. Fortuna, *Phys. Rev. B - Condens. Matter Mater. Phys.*, 2010, **81**, 45411.
64 Z. Vashaei, C. Bayram, P. Lavenus and M. Razeghi, *Appl. Phys. Lett.*, 2010, **97**, 121918.
65 L. Jonas, O. Brandt, C. Pf, T. Flissikowski, U. Jahn, E. Luna and M. Hanke, *Phys. Rev. B - Condens. Matter Mater. Phys.*, 2011, **84**, 155303.
66 Y. S. Chiu, M. H. Ya, W. S. Su and Y. F. Chen, *J. Appl. Phys.*, 2002, **92**, 5810–5813.
67 C. Weisbuch and B. Vinter, *Quantum Semiconductor Structures*, 1991.
68 J. M. Jancu, K. Gauthron, L. Largeau, G. Patriarche, J. C. Harmand and P. Voisin, *Appl. Phys. Lett.*, 2010, **97**, 2008–2011.
69 N. Vainorius, S. Lehmann, D. Jacobsson, L. Samuelson, K. A. Dick and M. Pistol, *Nano Lett.*, 2015, **15**, 2652.
70 M. Orrù, E. Repiso, S. Carapezzi, A. Henning, S. Roddaro, A. Franciosi, Y. Rosenwaks, A. Cavallini, F. Martelli and S. Rubini, *Adv. Funct. Mater.*, 2016, **26**, 2836–2845.
71 I. Dirnstorfer, M. T. Wagner, D. M. Hofmann, M. D. Lampert, F. Karg and B. K. Meyer, *phys. stat. sol. a*, 1998, **168**, 163–176.
72 A. Bauknecht, S. Siebentritt, J. Albert and M. C. Lux-steiner, *J. Appl. Phys.*, 2001, **89**, 4391–4400.
73 H. P. He, Z. Wang, H. F. Duan and Z. Z. Ye, *Phys. Chem. Chem. Phys.*, 2015, **17**, 17552–17556.
74 R. Pässler, *Phys. Status Solidi*, 1997, **200**, 155–172.
75 P. J. Dean, *Prog. Solid State Chem.*, 1973, **8**, 1–126.
76 P. M. P. Salomé, J. P. Teixeira, J. Keller, T. Törndahl, S. Sadewasser and J. P. Leit, *IEEE J. PHOTOVOLTAICS*, 2017, **7**, 670–675.
77 M. Murayarna and T. Nakayama, *Phys. Rev. B*, 1994, **49**, 4710.
78 C. E. Pryor, *Phys. Rev. B - Condens. Matter Mater. Phys.*, 2010, **81**, 155210.
79 M. Heiss, S. Conesa-Boj, J. Ren, H. H. Tseng, A. Gali, A. Rudolph, E. Uccelli, F. Peiro, J. R. Morante, D. Schuh, E. Reiger, E. Kaxiras, J. Arbiol and A. Fontcuberta I Morral, *Phys. Rev. B - Condens. Matter Mater. Phys.*, 2011, **83**, 45303.
80 A. P. Levanyuk and V. V Osipov, *Sov. Phys. Usp*, 1973, **7**, 721.
81 A. P. Levanyuk and V. V Osipov, *Sov. Phys. Usp*, 1973, **7**, 727.
82 B. Ketterer, M. Heiss, E. Uccelli, J. Arbiol and A. Fontcuberta, *ACS Nano*, 2011, **5**, 7585–7592.
83 T. B. Hoang, A. F. Moses, H. L. Zhou, D. L. Dheeraj, B. O. Fimland and H. Weman, *Appl. Phys. Lett.*, 2009, **94**, 133105.